Amphiphilic Ruthenium Sensitizer with 4,4′-Diphosphonic Acid-2,2′-bipyridine as Anchoring Ligand for Nanocrystalline Dye Sensitized Solar Cells

Peng Wang, Cédric Klein, Jacques-E. Moser, Robin Humphry-Baker, Ngoc-Le Cevey-Ha, Raphael Charvet, Pascal Comte, Shaik M. Zakeeruddin,* and Michael Grätzel*

Laboratory for Photonics and Interfaces, Swiss Federal Institute of Technology, CH-1015 Lausanne, Switzerland

Received: July 11, 2004; In Final Form: August 30, 2004

A new amphiphilic polypyridyl ruthenium complex, *cis*-Ru(dpbpy)(dnbpy)$(NCS)_2$ (dpbpy = 4,4′-diphosphonic acid-2,2′-bipyridine; dnbpy = 4,4′-dinonyl-2,2′-bipyridine), was synthesized and demonstrated as an efficient sensitizer. The sensitizer was characterized by NMR, voltammetry, ATR-FTIR, resonance Raman, as well as electronic absorption and emission spectra. Nanocrystalline dye-sensitized solar cells (DSCs) with this new sensitizer generated ≥8.0% power conversion efficiencies under illumination with simulated air mass 1.5 sunlight. This is the first time such a high solar-to-electricity power conversion efficiency for DSCs has been reached by a sensitizer bearing non-carboxylic acid anchoring groups. Additionally, the devices exhibited excellent stability under light soaking at 55 to 60 °C. Time-resolved nanosecond laser experiments revealed that the dye regeneration rate of this new sensitizer seems to be quite similar but the charge recombination is significantly slower in comparison to the analogues carboxylated sensitizer.

Introduction

Surface modification of wide band gap semiconductors by anchoring redox-active dyes offers attractive photoelectrochemical applications.[1] Nanocrystalline semiconductor films, in particular of TiO_2, have been proven to be a critical component in dye sensitized solar cells (DSCs) owing to their transparency, high surface area, and unique electronic properties. DSCs have significant potential as a low-cost alternative to conventional p−n junction solar cells.[2] Attachment of sensitizers on the surface of the TiO_2 allows for efficient electronic communication between the light-harvesting center and semiconductor substrate. Until now sensitizers based on polypyridyl ruthenium(II) complexes out-perform the metal-free organic sensitizers for solar power conversion. In this context, the most efficient sensitizers studied so far are some ruthenium complexes which can be chemisorbed on the TiO_2 surface via the carboxylate group.[3] An alternative anchoring group is the phosphonic acid that binds even more strongly onto TiO_2. Grafting sensitizers on the surface of TiO_2 with the phosphonic acid group has been reported earlier by us[4−6] and other groups.[7−13]

Recently, we have demonstrated the significance of using an amphiphilic polypyridyl ruthenium sensitizer to achieve unprecedented stability in DSCs at elevated temperatures.[14] Also, self-assembling of ω-alkylphosphonic acids on a wide range of metal oxide surfaces has been of great scientific and practical interest due to the ability to form robust and compact monolayers.[15−31] Hence, it is of great interest to design and synthesize amphiphilic ruthenium sensitizers containing the phosphonic acid group for dye sensitized solar cells. In this paper we report on the synthesis and photophysical and photoelectrochemical behavior of an amphiphilic sensitizer (coded as Z-955, Figure 1) endowed with 4,4′-diphosphonic acid-2,2-bipyridine (dpbpy) as the anchoring ligand. We show that such a rational sensitizer design enables good photovoltaic performances to be matched with very strong surface binding.

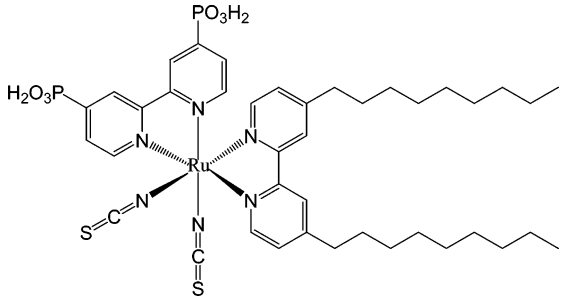

Figure 1. Molecular structures of the Z-955 dye.

Experimental Section

Regents and Electrolytes. All chemicals and solvents used were of puriss quality. [$RuCl_2$(*p*-cymene)$_2$], guanidinium thiocyanate, 4,4′-dinonyl-2,2′-bipyridine (dnbpy), and *N*-methylbenzimidazole (NMBI) were purchased from Aldrich. The latter was recrystallized from diethyl ether. 3-Methoxypropionitrile (MPN, Fluka) was distilled before use. Sephadex LH-20 was obtained from Pharmacia (Sweden). dpbpy was synthesized by following the published procedure.[12] Ionic liquids of 1-propyl-3-methylimidazolium iodide[32] (PMII), 1-ethyl-3-methylimidazolium bis(trifluoromethanesulfonyl)amide[33] (EMITFSI), and 1-ethyl-3-methylimidazolium thiocycante[34] (EMINCS) were prepared according to literature methods and their purities were confirmed by ^{1}H NMR spectra. The composition of the electrolytes was as follows: (A) 0.6 M PMII, 30 mM I_2, 0.1 M guanidinium thiocyanate, and 0.5 M *tert*-butylpyridine in the mixture of acetonitrile and valeronitrile (volume ratio 3/1);[35] (B) 0.6 M PMII, 0.1 M I_2, and 0.5 M NMBI in MPN;[36] and (C) 0.2 M I_2, 0.1 M guanidinium thiocyanate, and 0.5 M NMBI in the mixture of PMII and EMINCS (volume ratio 13/7).

* To whom correspondence should be addressed. E-mail: shaik.zakeer@epfl.ch and michael.graetzel@epfl.ch.

10.1021/jp046932x CCC: $27.50
Published on Web 10/15/2004

Synthesis of the Z-955 Dye. $RuCl_2(p\text{-cymene})_2$ (0.1 g, 0.16 mmol) and dnbpy (0.133 g, 0.32 mmol) were dissolved in DMF (50 mL). The reaction mixture was heated to 60 °C under nitrogen for 4 h with constant stirring. In a separate flask dbbpy (0.1 g, 0.32 mmol) was dissolved in 20 mL of methanol and titrated with a methanolic solution of tetra-*n*-butylammonium hydroxide to pH 4.5. After evaporating the solvent, the resulting solid redissolved in DMF (20 mL) was transferred to the above reaction mixture. After 4 h of refluxing, an excess of NH_4NCS (13 mmol) was added and the reflux continued for another 4 h. The reaction mixture was cooled to room temperature and the solvent was removed with a rotary evaporator under vaccum. Then, water was added to the flask and the insoluble solid was collected on a sintered glass crucible by suction filtration. Finally, the solid was dissolved in a basic methanolic solution and purified on a Sephadex LH-20 column by eluting with methanol. After complete acidification, the resulting compound was coded as Z-955 dye. ^{1}H NMR (δ_H/ppm in CD_3OD with NaOD): 9.5 (d, 1H), 9.3 (d, 1H), 8. 8 (d, 1H), 8.7 (d, 1H), 8.5 (s, 1H), 8.4 (s, 1H), 8.1 (d, 1H), 7.80 (d, 1H), 7.4 (m, 3H), 7.1 (d, 1), 3.0 (t, 2H), 2.8 (t, 2H), 1. 95 (m, 2H), 1.4 (m, 26H), 0.9 (t, 6H). ^{31}P NMR (δ_P/ppm in CD_3OD with NaOD): 7.88 and 8.83.

Spectroscopic Measurements. UV−vis electronic absorption and emission spectra were measured with a Cary 5 UV−vis−NIR spectrophotometer and a Spex Fluorolog 112 spectrofluorometer, respectively. The emitted light was detected with a Hamamatsu R2658 photomultiplier operated in a single-photon counting mode. The emission spectrum was photometrically corrected with a calibrated 200 W tungsten halogen lamp as reference source.

The FTIR spectra for all the samples were measured with a Digilab 7000 FTIR spectrometer. The ATR data reported here were taken with the "Golden Gate" diamond anvil ATR accessory (Graseby-Specac), using typically 64 scans at a resolution of 4 cm^{-1}. The samples were all measured under the same mechanical force pushing the samples in contact with the diamond window. No ATR correction has been applied to the data. It also has to be appreciated that this ATR technique probes at most 1 μm of sample depth and that this depends on the sample refractive index, porosity, etc. Some spectra show artifacts due to attenuation of light by the diamond window in the 2000−2350-cm^{-1} region of the spectrum.

The resonance Raman (RR) spectra were obtained with a Coherent INNOVA 200K Kr^+ laser source and a SPEX 1877 Triplemate with liquid N_2 cooled CCD-1024 detection. Excitation wavelengths were 468.041, 482.518, or 520.832 nm. All the data reported here were irradiated with use of a front face 135° scattering geometry. In this configuration, the laser beam waist at the sample was about 6 mm. The dye samples were measured on TiO_2 anatase films in the dry state and in a sealed DSC cell. Laser-induced sample degradation was minimized by applying low laser power (typically 10 mW) and by spinning the sample in the exciting laser beam. All the data are photometrically corrected with use of a standard 200 W halogen lamp. The spectral resolution was typically 2 cm^{-1}. Baseline correction has been applied to the displayed spectra.

Electrochemical, Photoelectrochemical, and Transient Absorbance Measurements. Cyclic voltammetry measurements were performed on a computer-controlled Autolab P20 electrochemical workstation (Eco Chimie, Netherlands) in combination with a conventional three-electrode, one-compartment electrochemical cell. A Pt foil and an $Ag/AgCl/KCl_{sat}$ were used as counter and reference electrodes, respectively. A dye-coated nanocrystalline TiO_2 electrode was employed as the working electrode. Due to the possible liquid junction potential, the reference electrode used was calibrated by measuring the redox potential of ferrocene dissolved in EMITFSI. The redox potentials referenced to calibrated $Ag/AgCl/KCl_{sat}$ were converted to the NHE reference scale. Photovoltaic behavior and laser transient absorbance were measured as described in our previous publications.[14,37]

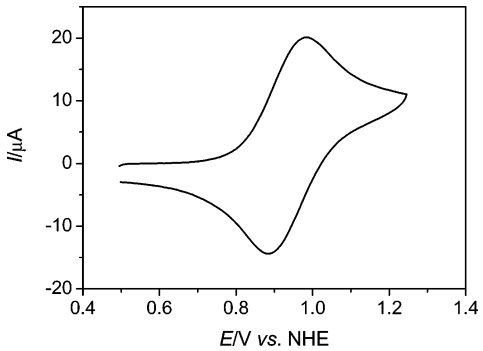

Figure 2. Cyclic voltammogram of a 6.5-μm-thich nanocrystalline TiO_2 electrode grafted with Z-955 dye in EMITFSI. The scan rate is 200 mV s^{-1}.

Device Fabrication. A double-layer TiO_2 mesoporous film was used as the photoanode. A 13 μm thick film of 20 nm TiO_2 particles was first printed on the fluorine-doped SnO_2 conducting glass electrode and further coated by a 4 μm thick second layer of 400 nm light scattering anatase particles. The detailed fabrication procedures for the nanocrystalline TiO_2 photoanodes and the assembly of complete, hot-melt sealed cells have been described elsewhere.[37] The TiO_2 electrodes were surface derivatized by immersing them into the dye solution of 300 μM Z-955 in acetonitrile and *tert*-butyl alcohol (volume ratio 1/1) at room temperature for 48 h. Devices with the Z-955 dye and electrolyte A (B or C) are denoted as device A (B or C). As a reference, device D is made with the Z-907 dye[14] and electrolyte B.

Stability Tests. Hermetically sealed cells were used for long-term stability tests under moderate thermal stress and visible light soaking. The cells were covered with a 50 μm thick polyester film (Preservation Equipment Ltd, UK) as a UV cutoff filter (up to 400 nm) and were irradiated at open circuit under a Suntest CPS plus lamp (ATLAS GmbH, 100 mW cm^{-2}, 55−60 °C).

Results and Discussion

Redox Behavior of the Z-955 Dye. One basic requisite for a sensitizer in regenerative dye-sensitized solar cells is that its formal redox potential of the ground state [$\phi^0(S^+/S)$] should be more positive than that of the iodide/triode couple in electrolytes. Thus we employed cyclic voltammetry to check the $\phi^0(S^+/S)$ of Z-955 anchored on TiO_2 nanocrystals. Figure 2 shows the typical cyclic voltammogram of 6.5 μm thick TiO_2 nanocrystalline film coated conducting glass electrode grafted with Z-955 dye in the EMITFSI ionic liquid which has a very broad electrochemical window.[33] When the potential is scanned between −0.2 and +1.15 V, chemically reversible redox waves with the formal potential, $(E_{ox} + E_{red})/2$, at 0.94 V are observed. These can be attributed to the one-electron oxidation and reduction of the ruthenium center of the Z-955 dye as the TiO_2 nanocrystalline film coated conducting glass has no electroactivity in the investigated potential range. The 100 mV peak−peak separation may be caused by the uncompensated ohmic drop in the electrolyte solution, slow direct electron transfer

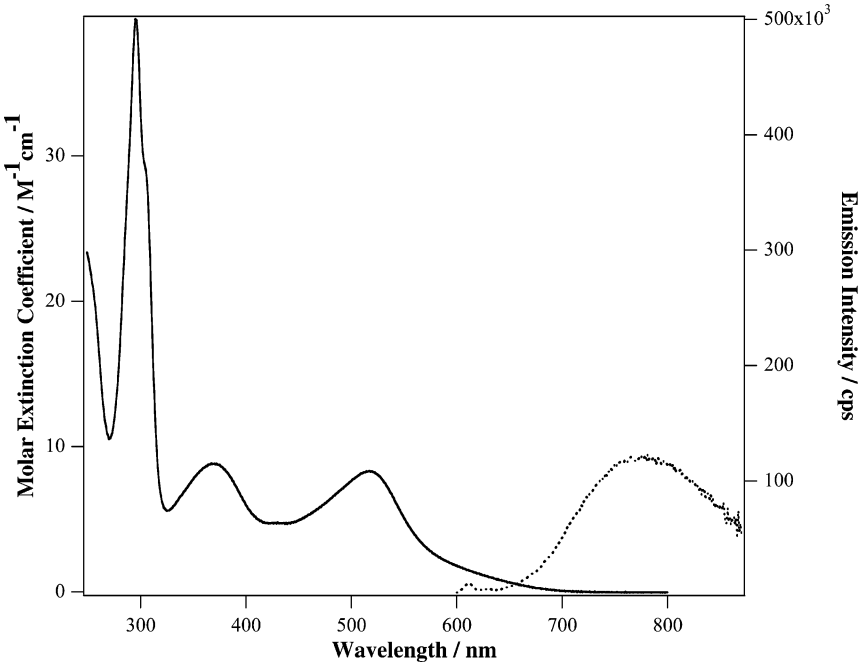

Figure 3. Electronic absorption and emission spectra of the Z-955 dye in ethanol.

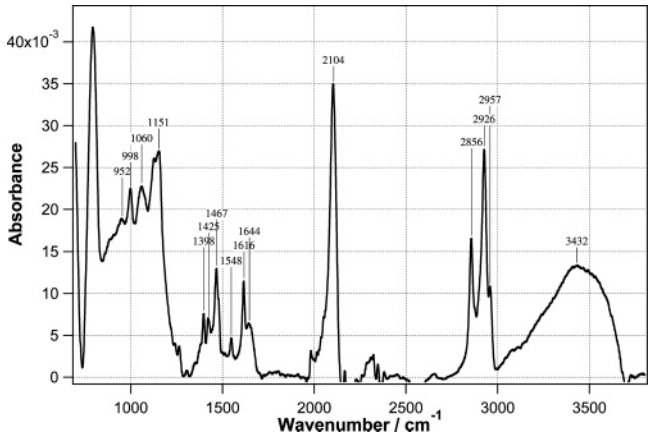

Figure 4. The ATR-FTIR spectrum for the 6.5 μm thick mesoporous TiO_2 film coated with the Z-955 dye. A TiO_2 reference film heated to 500 °C has been subtracted for clarity.

between the conducting glass and the Z-955 dye anchored onto the TiO_2 surface, or slow electrostatic charge compensation during the redox process.

Spectroscopy. Figure 3 shows the electronic absorption spectrum and emission spectrum of the Z-955 in an alcoholic solution. The absorption spectrum shows the usual MLCT maxima at 519 and 370 nm. These bands tail off toward 750 nm, contributing to the broad spectral light harvesting that is characteristic of polypyridyl ruthenium dyes. The ligand $\pi \rightarrow \pi^*$ bands are found further to the blue at 295 nm with a shoulder at 305 nm. The structureless MLCT emission is centered at 780 nm with an emission quantum yield of about $1(\pm 5\%) \times 10^{-3}$ with quinine sulfate as a reference.[38]

The ATR-FTIR spectrum of the Z-955 dye on the surface of anatase is shown in Figure 4. The ATR technique shows clearly the presence of Z-955 on the surface, the characteristic vibrational transitions of the C-9 alkyl chains being observed at 1467, 2856, 2926, and 2959 cm^{-1}. The position and line widths of the $\nu_s(CH_2)$ and $\nu_a(CH_2)$ peaks are diagnostics for the degree of ordering in a monolayer. The methylene peak positions and peak width are typical for other dyes functionalized with hydrophobic alkyl chains such as the Z-907 dye.[36,37] The peaks at 1398, 1548, and 1615 cm^{-1} are ring modes due to the bipyridyl ligand. The strong thiocyanate band due to the $-CN$ stretch is identifiable at 2104 cm^{-1}. The PO_3H_2 attachment group of the Z-955 dye displays moderately strong peaks in the 900 to 1200 cm^{-1} region prior to surface attachment. The strong band at 929 cm^{-1} probably involves the $P-OH$ stretch, while the $P-O^-$ symmetric and asymmetric absorption are seen at 1150 cm^{-1}. Upon adsorption onto the TiO_2 surface the strong $P-OH$ band disappears and is replaced by weaker peaks at 952 and 1060 cm^{-1}. The $P-O^-$ feature is still seen but shifted slightly to 1151 cm^{-1}. The peaks seen at 1060 cm^{-1} and the shoulder at 1129 cm^{-1} are indicative of the phosphonate symmetric and asymmetric modes that are implicated in the surface binding.[39]

Previously, Hagfeldt et al.[40,41] have used in situ resonance Raman scattering to scrutinize the possible coordinative interactions of main chemical components in dye sensitized solar cells. The resonance Raman spectrum shown in Figure 5 is employed to directly observe the Z-955 dye attached to the anatase surface in a sealed DSC with electrolyte B. By using the 520.8 nm laser excitation, the three strong ring modes of the ligand can be readily identified with features at 1468, 1521, and 1604 cm^{-1}. Normally these three strong signals are representative of the ligand implicated in the lowest energy MLCT electronic transistion.[42] Other ring modes are seen at 1021 and 721 cm^{-1}. Since Z-955 is a heteroleptic complex, there are two possible ligands that can be excited at this wavelength. Closer inspection of Figure 5 shows that each ring mode is a doublet with contributions from both the dpbpy and dnbpy ligands. By comparing the spectrum with the $Ru(dpbpy)_3Cl_2$ reference compound, the peaks due to the dpbpy ligand can be assigned to 1474, 1521, and 1604 cm^{-1}. The dnbpy ligand is identified from marker bands at 1468, 1536, and 1609 cm^{-1}. By probing the resonance Raman spectra produced by 482.5 and 468.0 nm excitation, the contribution of the dnbpy ligand becomes more important. This would suggest that the phosphonated ligand (dpbpy) has a slightly lower π^* level compared to the dnbpy ligand. Semiempirical molecular orbital calculation has also

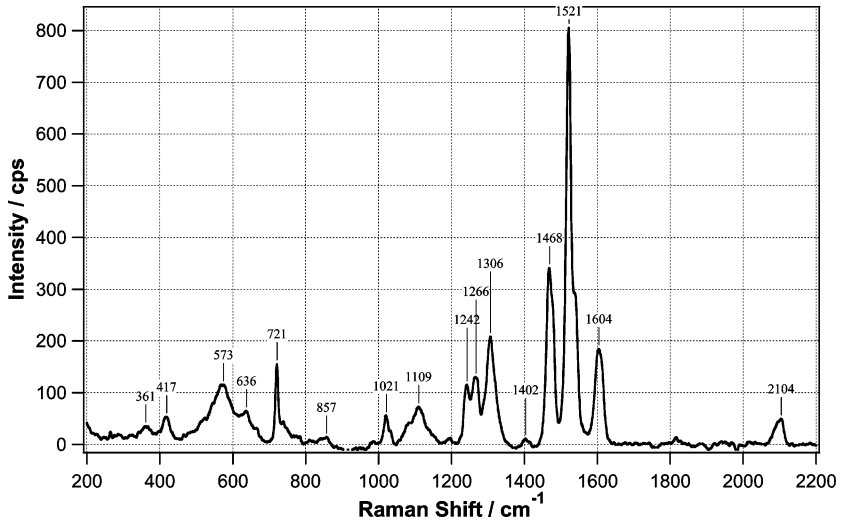

Figure 5. Resonance Raman spectrum of device B with the Z-955 dye. The excitation wavelength is 520.8 nm.

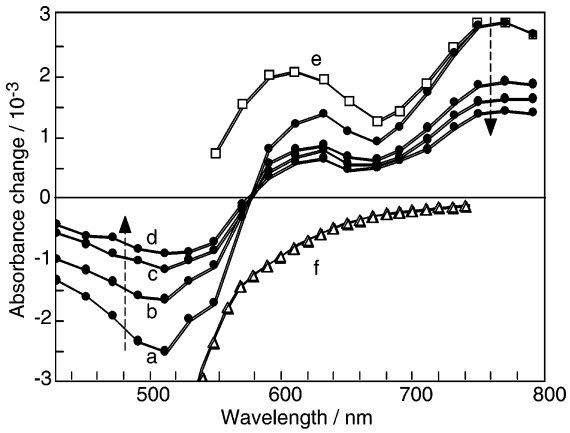

Figure 6. Transient absorbance spectra of Z-955 dye adsorbed on a nanocrystalline TiO_2 film in pure MPN solvent, recorded 20 (a), 50 (b), 200 (c), and 500 μs (d) after pulsed laser excitation of the sensitizer (540 nm excitation wavelength, 5 ns fwhm pulse duration, 100 μJ cm^{-2} pulse fluence). The absorption spectrum of the oxidized state of Z-955 (e) was obtained from raw transient spectra by subtracting the contribution of the bleaching of the dye ground state (f).

indicated that the dpbpy π^* is lower in energy than the corresponding dnbpy π^*. This requirement is essential for vectorial electron transfer to occur from the sensitizer via the attachment group into the TiO_2 conduction band. Contrary to the IR spectrum, the thiocyanate Raman mode at 2097 cm^{-1} is weak.

Laser Transient Kinetics. To a large extent the photon-to-current conversion efficiency of DSCs is controlled by the kinetic competition between back electron transfer of injected electrons from the TiO_2 conduction band to the oxidized dye cations (S^+) and the interception of S^+ by the redox mediator. Hence, it is very valuable to scrutinize the dynamics of these charge-transfer processes for the new sensitizer with time-resolved nanosecond laser experiments. The fluence at the sample of excitation laser pulses at 540 nm was limited in all experiments to 50−100 μJ cm^{-2} to ensure that, on average, less than one electron is injected per nanocrystalline TiO_2 particle on pulsed irradiation.

Figure 6 shows the time evolution of the transient absorption spectra of Z-955 anchored on the mesoprous TiO_2 film in the presence of pure MPN solvent upon pulsed laser excitation. The features are shifted to shorter wavelengths compared to those obtained with the standard N-719 dye.[43,44] In particular, the isobestic point is located at 575 nm, which is 20 nm blue-shifted compared with that of the N-719 dye. The positive absorption feature observed above 580 nm is assigned to a ligand-to-metal charge transfer (LMCT) transition from the thiocyanate ligand to the Ru(III) center of the oxidized form of Z-955 (S^+) produced by subpicosecond charge injection.[45] Transient spectra were corrected by subtracting the contribution of the bleaching of the dye ground state: The employed laser pulse fluence of 100 μJ cm^{-2} corresponded to the absorption of 2.6×10^{14} photons/cm^2 in dye-sensitized sample films, characterized typically by an absorbance of 1.2, and hence to the excitation of 4.2×10^{-10} mol/cm^2 of the sensitizer. By using a value of 7×10^3 M^{-1} cm^{-1} for the extinction coefficient of the dye at 540 nm, the bleaching of the ground state was estimated to yield an absorbance change of 3×10^{-3} at this wavelength. The resulting corrected spectrum shown in Figure 6e exhibits two absorption bands peaking approximately at 600 and 770 nm. The first band is obviously responsible for the peak around 640 nm observed in the transient spectra. This feature is not apparent in the transient spectrum measured with N-719, most probably due to the higher extinction coefficient characterizing this dye in this wavelength region. The broad absorption band in the red observed in Figure 6 is clearly blue shifted compared to the spectrum of the oxidized N-719. We note the expected correlation between the energy of the LMCT transition of the oxidized species of the analogous complexes N-719, Z-955, and *cis*-Ru(bpy)$_2$(NCS)$_2$, whose absorptions peak at ~790, 770, and 746 nm, respectively, and their standard redox potentials (1.13, 0.94, and 0.78 V vs NHE, respectively).[44,46]

In the absence of electron donor, the decay of the absorption signal recorded at 650 nm reflects the dynamics of recombination of injected electrons with the oxidized dye (S^+). The kinetics of S^+ transient absorbance decay displayed a typical half-reaction time $t_{1/2} = 800$ μs (Figure 7, trace a). Charge recombination under these conditions is significantly slower than that for the analogous Z-907 dye, for which $t_{1/2} = 180$ μs was reported in our previous work.[14] Because these two sensitizers have the same redox center, the slower recombination is ascribed to a decrease of the electronic coupling between the Ti 3d orbitals and the dye cation S^+ when the carboxylic anchoring groups are replaced by the phosphonate groups. In the presence of electrolyte B, the decay of the oxidized dye signal was significantly accelerated with $t_{1/2} = 10$ μs, showing that back electron transfer was indeed efficiently intercepted by the iodide electron donor (Figure 7, trace b). The dye regeneration in the

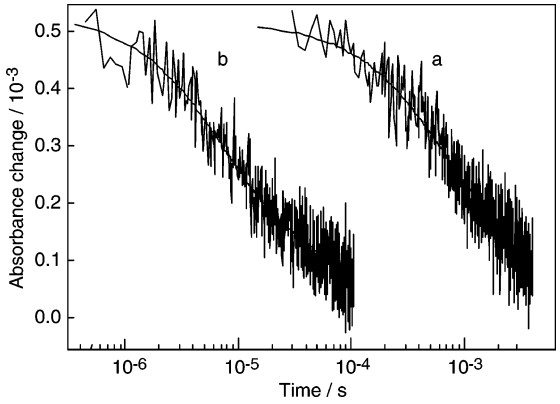

Figure 7. Transient absorbance decay kinetics of the oxidized state of Z-955 dye adsorbed on a nanocrystalline TiO_2 film in pure MPN solvent (a) and in the presence of Z-208 electrolyte (b). Absorbance changes were measured at a probe wavelength of 650 nm, employing 540 nm laser excitation (5 ns fwhm pulse duration, 50 μJ cm^{-2} pulse fluence).

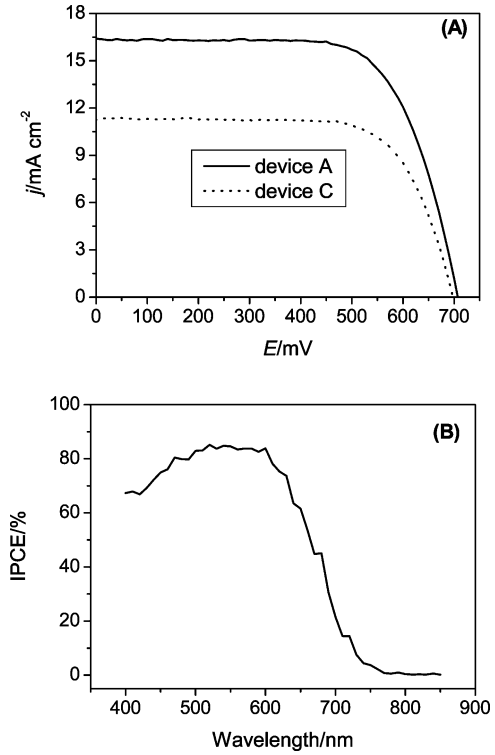

Figure 8. (A) Photocurrent density−voltage characteristics of device A and device C under air mass 1.5 (100 mW cm^{-2}) illumination. (B) Photocurrent action spectrum of device A. The active area of devices with a mask is 0.158 cm^2.

presence of iodide redox electrolyte appears to occur within the same time frame as that for the Z-907 dye ($t_{1/2}$ = 5−30 μs).

Photovoltaic Performance. Figure 8A presents the current−voltage characteristics of device A and device C illuminated with air mass (AM) 1.5 simulated solar light at 100 mW cm^{-2}. Table 1 summarizes device performances at different light intensities. The short circuit current density (J_{sc}), open circuit voltage (V_{oc}), fill factor (ff), and power conversion efficiency (η) of device A were measured to be 16.37 mA cm^{-2}, 707 mV, 0.693, and 8.0%, respectively. This is the first time such a high efficiency has been achieved by a ruthenium complex endowed with an anchoring group other than carboxylate between the light-harvesting components and oxide semiconductors. The excellent electron injection of Z-955 dye can be seen from

TABLE 1: Device Efficiencies of DSCs at Varied Sunlight Irradiation

	η (%) at different light intensities[a]		
device	0.1 Sun	0.5 Sun	1.0 Sun
A	8.4	8.2	8.0
B	6.5	6.8	6.4
C	6.0	6.0	5.5

[a] The spectral distribution of the lamp simulates air mass 1.5 solar light. 1.0 Sun corresponds to an intensity of 100 mW cm^{-2}.

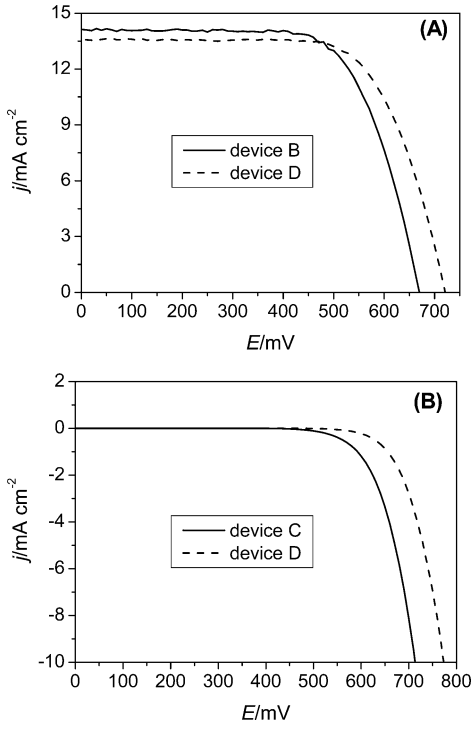

Figure 9. (A) Photocurrent density−voltage characteristics of device B with the Z-955 dye and device D with the Z-907 dye under an illumination of air mass 1.5 sunlight at 100 mW cm^{-2}. (B) The plot of dark current density versus negative bias potential. The active area of devices with a mask is 0.158 cm^2.

Figure 8B. For device C employing a solvent-free, binary ionic liquid electrolyte, the corresponding device parameters (J_{sc}, V_{oc}, ff, and η) are 11.3 mA cm^{-2}, 0.70 V, 0.709, and 5.5%, respectively. With the latter system, 6% power conversion efficiencies have been reached at low incident intensities, which are more close to the practical light conditions for the application of plastic matrix-based flexible dye sensitized solar cells.

To further evaluate its photovoltaic performance compared with the Z-907 dye in DSCs, a standard electrolyte with MPN as solvent was used for the fabrication of device B. As shown in Figure 9A, its photovoltaic parameters (J_{sc}, V_{oc}, ff, and η) under standard air mass 1.5 sunlight (100 mW cm^{-2}) are 14.12 mA cm^{-2}, 670 mV, 0.681, and 6.4%, respectively. Keeping in mind the corresponding photovoltaic parameters[36] (J_{sc} of 13.6 mA cm^{-2}, V_{oc} of 721 mV, ff of 0.692, and η of 6.8%) of device D employing the Z-907 dye, it appears that ruthenium sensitizers endowed with the phosphonate anchoring group can match the performance of carboxylated analogues.

If we assume that there is a very similar packing mode for Z-907 and Z-955 dye molecules on TiO_2 except for the different anchoring group, the more negative onset potential (Figure 9B) for the dark current curve of device D compared with device B indicates that the flat-band potential of the nanocrystalline TiO_2 film derivtized with Z-955 is more positive. Specific adsorption

of small cations onto oxide semiconductors is known to possibly modify surface charge, band-edge positions, and the energy level distribution of surface states.[47,48] The flat-band potential of the semiconductor in a dry aprotic electrolyte can be shifted to considerably more positive values upon adsorption of potential-determining ions such as protons or lithium ions.[49] Because during the staining step more protons are possibly introduced to the mesoporous TiO_2 film with Z-955 than Z-907, a decrease in V_{oc} by ca. 51 mV partially compensated by a rise in J_{sc} was observed.

It also should be noted that the blue-shifted spectral response of Z-955 dye compared with Z-907 should decrease the light-harvesting capacity and thus lower the J_{sc}. The fact that device B actually showed a larger J_{sc} is in keeping with the notion of the increased protonation of the TiO_2 surface by the Z-955, which carries four protons as opposed to two protons for Z-907.

Device Stability. As presented in Figure S1 of the Supporting Information, device B showed a good stability when submitted to the accelerated testing in a solar simulator with a 100 mW cm^{-2} light irradiance. After 1000 h of light soaking at 55 °C there is no drop of device efficiency for cells covered with a UV absorbing polymer film. During the aging process, a small fluctuation in open-circuit potential should be mainly related to the flat-band potential variation of the mesoporous film. In essence, during the dye staining step, protons released by dye-grafting or from the dye molecules can be adsorbed on the surface of the ungrafted region of TiO_2. However, during the initial 72 h of aging the imidazolium cations in the electrolyte might slowly replace the surface protons to some extent, resulting in an increase in device photovoltage. It seems that the subsequent thermal stress at 55 °C has reversed this surface reaction. Additionally, the initial enhancement of the device fill factor is due to a decrease in serial resistance. While the activity of the platinized counter electrode, the electrolyte conductivity, and the resistance of the current collector are not expected to change, the decreased resistance should be mainly caused by the charge-transfer impedance in the interface between the dye-coated nanocrystals and electrolyte.

Room temperature ionic liquid electrolytes have been actively pursued as nonvolatile electrolytes of DSCs, but only very recently did a binary electrolyte of EMISCN and PMII allow us to achieve acceptable device stabilities under light soaking at moderate thermal stress.[50] As shown in Figure S2 of the Supporting Information, device C demonstrated a very excellent light soaking stability. After 1000 h of aging tests, the device efficiency only changed from 5.5% to 5.4%. The <40 mV drop in open-circuit photovoltage was compensated by the increase of short-circuit photocurrent density from 11.26 to 11.78 mA cm^{-2} while the fill factor is considerably stable. This is the first time such a good stability has been achieved for DSCs with solvent-free ionic liquid electrolytes.

Conclusions

A new amphiphilic polypyridyl ruthenium sensitizer with two phosphonic acid anchoring groups was synthesized and successfully used for dye-sensitized solar cells with a total power conversion efficiency of $\geq 8.0\%$ under simulated air mass 1.5 sunlight. This is the first time such a high solar-to-electricity power conversion efficiency in DSCs has been achieved by a sensitizer with non-carboxylic acid anchoring groups. Additionally, this new sensitizer has excellent light soaking stabilities at moderate temperature stress in the presence of both 3-methoxypropionitrile-based and solvent-free ionic liquid electrolytes.

Acknowledgment. The Swiss Science Foundation, Swiss Federal Office for Energy (OFEN), and the European Office of U.S. Air Force under Contract No. F61775-00-C0003 have supported this work.

Supporting Information Available: Detailed photovoltaic parameter evolution of devices B and C during the successive visible light soaking at 55∼60 °C. This material is available free of charge via the Internet at http://pubs.acs.org.

References and Notes

(1) Grätzel, M. *Nature* **2001**, *414*, 338.
(2) O'Regan, B.; Grätzel, M. *Nature* **1991**, *353*, 737.
(3) Grätzel, M. *J. Photochem. Photobiol. A: Chem.* **2004**, *164*, 3.
(4) Péchy, P.; Rotzinger, F. P.; Nazeeruddin, M. K.; Kohle, O.; Zakeeruddin, S. M.; Humphry-Baker, R.; Grätzel, M. *J. Chem. Soc., Chem. Commun.* **1995**, 65.
(5) Ruile, S.; Kohle, O.; Péchy, P.; Grätzel, M. *Inorg. Chim. Acta* **1997**, *261*, 129.
(6) Zakeeruddin, S. M.; Nazeeruddin, M. K.; Pechy, P.; Rotzinger, F. P.; Humphry-Baker, R.; Kalyanasundaram, K.; Grätzel, M. *Inorg. Chem.* **1997**, *36*, 5937.
(7) Yan, S. G.; Hupp, J. T. *J. Phys. Chem.* **1996**, *100*, 6867.
(8) Yan, S. G.; Prieskorn, J. S.; Kim, Y.; Hupp, J. T. *J. Phys. Chem. B* **2000**, *104*, 10871.
(9) Trammell, S. A.; Wimbish, J. C.; Odobel, F.; Gallagher, L. A.; Narula, P. M.; Meyer, T. J. *J. Am. Chem. Soc.* **1998**, *120*, 13248.
(10) Trammell, S. A.; Moss, J. A.; Yang, J. C.; Nakhle, B. M.; Slate, C. A.; Odobel, F.; Sykora, M.; Erickson, B. W.; Meyer, T. J. *Inorg. Chem.* **1999**, *38*, 3665.
(11) Zimmermann, C.; Willig, F.; Ramakrishna, S.; Burfeindt, S.; Pettinger, B.; Eichberger, R.; Storck, W. *J. Phys. Chem. B* **2001**, *105*, 9245.
(12) Gillaizeau-Gauthier, I.; Odobel, F.; Alebbi, M.; Argazzi, R.; Costa, E.; Bignozzi, C. A.; Qu, P.; Meyer, G. J. *Inorg. Chem.* **2001**, *40*, 6073.
(13) Zabri, H.; Gillaizeau, I.; Bignozzi, C. A.; Caramori, S.; Charlot, M.-F.; Cano-Boquera, J.; Odobel, F. *Inorg. Chem.* **2003**, *42*, 6655.
(14) Wang, P.; Zakeeruddin, S. M.; Moser, J. E.; Nazeeruddin, M. K.; Sekiguchi, T.; Grätzel, M. *Nat. Mater.* **2003**, *2*, 402.
(15) Yang, H. C.; Aoki, K.; Hong, H.-C.; Sackett, D. D.; Arendt, M. F.; Yau, S.-L.; Bell, C. M.; Mallouk, T. E. *J. Am. Chem. Soc.* **1993**, *115*, 11855.
(16) Hong, H.-G.; Mallouk, T. E. *Langmuir* **1991**, *7*, 2362.
(17) Gardner, T. J.; Frisbie, C. D.; Wrighton, M. S. *J. Am. Chem. Soc.* **1995**, *117*, 6927.
(18) Folkers, J. P.; Gorman, C. B.; Laibinis, P. E.; Buchholz S.; Whitesides, G. M.; Nuzzo, R. G. *Langmuir* **1995**, *11*, 813.
(19) Gao, W.; Reven, L. *Langmuir* **1995**, *11*, 1860.
(20) Gao, W.; Dickinson, L.; Grozinger, C.; Morin, F. G.; Reven, L. *Langmuir* **1996**, *12*, 6429.
(21) Gao, W.; Dickinson, L.; Grozinger, C.; Morin, F. G.; Reven, L. *Langmuir* **1997**, *13*, 116.
(22) Badia, A.; Lennox, R. B.; Reven, L. *Acc. Chem. Res.* **2000**, *33*, 475.
(23) Pawsey, S.; Yach, K.; Reven, L. *Langmuir* **2002**, *18*, 5205.
(24) Pawsey, S.; McCormick, M.; De Paul, S.; Graf, R.; Lee, Y. S.; Reven, L.; Spiess, H. W. *J. Am. Chem. Soc.* **2003**, *125*, 4174.
(25) Yim, C. T.; Pawsey, S.; Morin, F. G.; Reven, L. *J. Phys. Chem. B* **2002**, *106*, 1728.
(26) Pawsey, S.; Yach, K.; Halla, J.; Reven, L. *Langmuir* **2000**, *16*, 3294.
(27) Hanson, E. L.; Schwartz, J.; Nickel, B.; Koch, N.; Danisman, M. F. *J. Am. Chem. Soc.* **2003**, *125*, 16074.
(28) Gawalt, E. S.; Avaltroni, M. J.; Koch, N.; Schwartz, J. *Langmuir* **2001**, *17*, 5736.
(29) Gawalt, E. S.; Lu, G.; Bernasek, S. L.; Schwartz, J. *Langmuir* **1999**, *15*, 8929.
(30) Pellerite, M. J.; Dunbar, T. D.; Boardman, L. D.; Wood, E. J. *J. Phys. Chem. B* **2003**, *107*, 11726.
(31) Merrins, A.; Marguerettaz, X.; Rao, S. N.; Fitzmaurice, D. *Chem. Eur. J.* **2001**, *7*, 1309.
(32) Wang, P.; Zakeeruddin, S. M.; Comte, P.; Exnar, I.; Grätzel, M. *J. Am. Chem. Soc.* **2003**, *125*, 1166.
(33) Bonhôte, P.; Dias, A. P.; Armand, M.; Papageorgiou, N.; Kalyanasundaram, K.; Grätzel, M. *Inorg. Chem.* **1996**, *35*, 1168.
(34) Pringle, J. M.; Golding, J.; Forsyth, C. M.; Deacon, G. B.; Forsyth, M.; MacFarlane, D. R. *J. Mater. Chem.* **2002**, *12*, 3475.
(35) Wang, P.; Zakeeruddin, S. M.; Moser, J. E.; Humphry-Baker, R.; Comte, P.; Aranyos, V.; Hagfeldt, A.; Nazeeruddin, M. K.; Grätzel, M. *Adv. Mater.* **2004**, *16*, in press.
(36) Wang, P.; Zakeeruddin, S. M.; Humphry-Baker, R.; Moser, J. E.; Grätzel, M. *Adv. Mater.* **2003**, *15*, 2101.

(37) Wang, P.; Zakeeruddin, S. M.; Comte, P.; Charvet, R.; Humphry-Baker, R.; Grätzel, M. *J. Phys. Chem. B* **2003**, *107*, 14336.
(38) Parker, C. A. *Photoluminescence in Solution*; Elsevier: Amsterdam, The Netherlands, 1968.
(39) Undabeytia, T.; Morillo, E.; Maqueda, C. *J. Agric. Food Chem.* **2002**, *50*, 1918.
(40) Greijer, H.; Lindgren, J.; Hagfeldt, A. *J. Phys. Chem. B* **2001**, *105*, 6314.
(41) Agrell Greijer, G.; Lindgren, J.; Hagfeldt, A. *J. Photochem. Photobiol. A*: *Chem.* **2004**, *164*, 23.
(42) Strommen, D. P.; Mallick, P. K.; Danzer, G. D.; Lumpkin, R. S.; Kincaid, J. R. *J. Phys. Chem.* **1990**, *94*, 1352.
(43) Pelet, S.; Moser J. E.; Grätzel, M. *J. Phys. Chem. B* **2000**, *104*, 1791.
(44) Moser, J. E.; Noukakis, D.; Bach, U.; Tachibana, Y.; Klug, D. R.; Durrant, J. R.; Humphry-Baker, R.; Grätzel, M. *J. Phys. Chem. B* **1998**, *102*, 3649.
(45) Tachibana, Y.; Moser, J. E.; Grätzel, M.; Klug, D. R.; Durrant, J. R. *J. Phys. Chem.* **1996**, *100*, 200560.
(46) Kalyanasundaram, K.; Zakeeruddin, S. M.; Nazeeruddin, M. K. *Coord. Chem. Rev.* **1994**, *132*, 259.
(47) Wang, P.; Zakeeruddin, S. M.; Moser, J.-E.; Grätzel,M. *J. Phys. Chem. B* **2003**, *107*, 13280.
(48) Heller, A. *Acc. Chem. Res.* **1981**, *14*, 154.
(49) Haque, S. A.; Tachibana, Y.; Willis, R. L.; Moser, J. E.; Grätzel, M.; Klug, D. R.; Durrant, J. R. *J. Phys. Chem. B* **2000**, *104*, 538.
(50) Wang, P.; Zakeeruddin, S. M.; Humphry-Baker, R.; Grätzel, M. *Chem. Mater*. **2004**, *16*, 2694.